Atomic-scale control of plasmon modes in graphene nanoribbons

François Aguillon, Dana Codruta Marinica, Andrei Borisov

Letter

Atomic-scale control of plasmon modes in graphene nanoribbons

François Aguillon, Dana Codruta Marinica, and Andrei G. Borisov*
Institut des Sciences Moléculaires d'Orsay (ISMO), UMR 8214, CNRS, Université Paris-Saclay, bât 520, Orsay Cedex, France

(Received 25 October 2021; revised 18 January 2022; accepted 19 January 2022; published 1 February 2022)

We address the possibility of atomic-scale control of the plasmon modes of graphene nanostructures. Using the time-dependent many-body approach we show that for the zigzag and armchair nanoribbons, the single carbon atom vacancy results in "on" and "off" switching of the longitudinal plasmon modes or in a change of their frequency. The effect stems from the robust underlying physical mechanism based on the strong scattering of the two-dimensional (2D) electrons on the vacancy defects in graphene lattice. Thus our findings establish a platform for optical response engineering or sensing in 2D materials.

DOI: 10.1103/PhysRevB.105.L081401

Control of the light-matter interactions is at the focus of many research areas because of the fundamental challenge and multiple practical applications ranging from attosecond pulse generation and energy harvesting, to metamaterials and (biological) sensors [1–7]. Since the electromagnetic response of the matter is strongly enhanced when the incident electromagnetic wave couples to collective electronic excitations, plasmons, one of the efficient routes of such control is the plasmon mode engineering. For metallic nanostructures, experimental and theoretical studies reported various strategies to modify the energies, lifetimes, and near -fields of the plasmon modes. These strategies imply adjusting the geometry of the individual nanoparticles, their arrangements into hybrid structures, electrochemistry, or changing the refractive index of the environment [8–15]. The two-dimensional (2D) materials, such as graphene, offer the unprecedented possibility of versatile and reversible active tuning of the plasmon modes via the charge doping [16–19].

Along with these successful developments, an ever growing demand for miniaturization puts forward a question of the possibility to modify an optical response by introducing changes at atomic scale. In this respect, it has been demonstrated that the changes in the atomic-scale conductive bridge between metallic nanostructures can affect plasmon response of the compound system [20–23]. As well, we know from molecular spectroscopy that the removal or substitution of a single atom changes the optical spectrum of a molecule. However, for the plasmon modes to be developed, the nanostructures have to comprise hundred(s) and even thousand(s) of atoms. Would it be possible to control the collective plasmon modes by single atom manipulation in such a case?

In this work, using the time-dependent tight-binding approach (TDTB) we show that the longitudinal plasmon modes of graphene nanoribbons (GNRs) are sensitive to a single carbon atom vacancy. By setting the defect position, a given plasmon mode can be switched "on" and "off" or shifted in energy. The effect is robust and it is caused by an efficient 2D electron scattering by vacancy defects in the nanoribbon geometry. Our study thus shows that, along with engineering of the conductivity and magnetic properties [24–32] of GNRs, introducing the atomic-scale changes within graphene lattice can also be used for the plasmon mode engineering of GNRs. This opens new perspectives for the creation of graphene-based plasmonic nanostructures for the far- and near-field manipulation by and for controlling a quantum emitter (QE) radiation.

The GNRs studied in this work are sketched in Fig. 1. They essentially consist of an ideal (defect-free) graphene lattice with a unique vacancy modeled by removing a single carbon atom. This simplified description of realistic vacancies [34–36] is often used in the literature as a representative example allowing one to grasp the underlying physics [25–28,37–43]. The vacancy position is defined by its coordinate along the x axis, x_v, and the number of the carbon atom row containing the vacancy, N_v. We consider armchair (AGNR-N) and zigzag (ZGNR-N) GNRs oriented along the x direction. The nanoribbon width is set by the number N of the carbon atom rows. Typically, the length of GNRs is $L \sim 20$ nm so that the nanostructures comprise $\sim 10^3$ carbon atoms. In this situation the longitudinal plasmon modes with induced currents along the x direction are well developed for the electronically doped ZGNRs and for the neutral AGNRs, as considered here in the main text [44–51]. Additionally, in the Supplemental Material (SM) [52] we show that the vacancy effects on the plasmon modes are similar for the neutral and electronically doped AGNRs. As indicated in Fig. 1, to "probe" the plasmon modes we excite the system with an x-polarized electromagnetic plane wave or with the QE represented by the point dipole $\mathbf{d}$ oriented along the x axis. Along with a characterization of the plasmon modes, using a point dipole source allows a discussion of the Purcell factor determining the rate of the decay of the quantum emitter in the vicinity of the nanoantenna.

The electron density dynamics in response to an external perturbation is obtained in real time from the self-consistent calculations based on the tight-binding description of the electronic structure of the π and π^* bands of graphene.

*andrei.borissov@universite-paris-saclay.fr

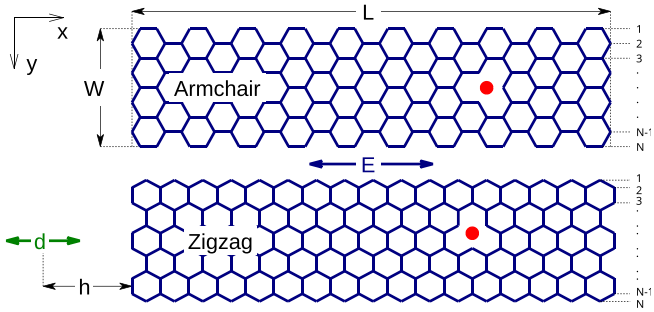

FIG. 1. Geometry of the studied armchair and zigzag graphene nanoribbons. Their width, W, is set by the number of graphene atomic rows, N, as defined on the right of the figure. The x coordinate is measured from the middle of the nanoribbon ($-L/2 \leqslant x \leqslant L/2$), and the y coordinate is measured from the first atomic row ($0 \leqslant y \leqslant W$). The vacancy is represented with a red dot. The system is excited by the electromagnetic x-polarized plane wave or by a quantum emitter represented by an x-oriented point dipole, d, located in the GNR plane at the left side of the GNR, at $h = 1$ nm and $y = W/2$.

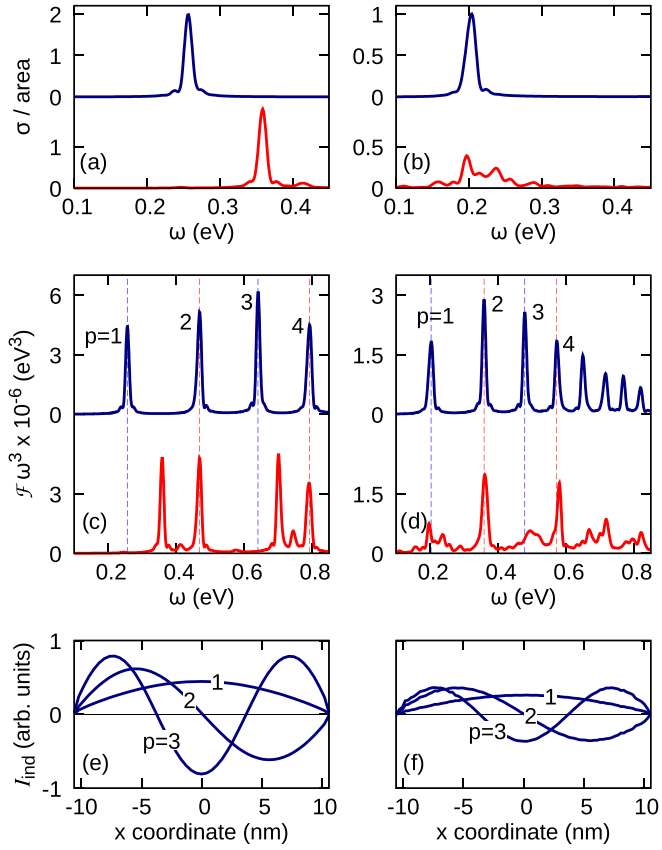

FIG. 2. Optical response of the AGNR-11 [panels (a),(c),(e)], and ZGNR-12 [panels (b),(d),(f)]. An artificial broadening of the spectra by 5 meV is applied [33]. The ZGNR-12 is electronically doped to Fermi energy $E_F = 0.4$ eV, while the AGNR-11 is neutral ($E_F = 0$). The blue curves in panels (a)–(d) correspond to the ideal GNRs. The red curves correspond to defective GNRs with the single carbon atom vacancy at $x_v = 0.07$ nm, $N_v = 5$ (AGNR-11), and at $x_v = 0.12$ nm, $N_v = 6$ (ZGNR-12). (a),(b) The optical absorption cross section σ of the GNRs. Results are shown as a function of the frequency of the incident electromagnetic plane wave. (c),(d) The decay rate enhancement $\mathcal{F} \times \omega^3$ ($\mathcal{F}$ is the Purcell factor) for the QE with transition frequency ω located in the vicinity of GNRs as indicated in Fig. 1. The resonances are labeled with p in order of increasing energy. (e),(f) The x-dependent induced currents $I_{\mathrm{ind},p}(x)$ associated with plasmon modes p.

Essentially, the present TDTB method is equivalent to the well established model descriptions used for graphene plasmonics [53,54], where the retardation effects are neglected owing to the small size of the system. The details of the present technique can be found elsewhere [55], and a short summary is given in the SM.

We first consider the situations where the carbon atom vacancy is introduced at the middle of the metallic [36,56] AGNR-11, and ZGNR-12 (see SM for the electronic structure of GNRs). The corresponding absorption spectra are shown in Figs. 2(a) and 2(b). For an ideal (defect-free) GNR the absorption cross section is dominated by the dipolar plasmon resonance. In agreement with previous studies, the absorption resonance is less pronounced for the ZGNR-12 because of the larger rate of the plasmon decay via Landau damping [45,48]. Strikingly, the single carbon atom vacancy strongly affects the optical response. For the AGNR-11 the energy of the dipolar plasmon resonance is blueshifted by 0.1 eV. For the ZGNR-12 the plasmon resonance is broadened by ∼0.4 eV so that it is essentially quenched [33].

The plane wave excitation reveals only the dipolar plasmon modes. That is why we also use the point dipole excitation which "probes" the density of the electromagnetic states of the system and thus the multipolar plasmon modes [57–59]. In Figs. 2(c) and 2(d) we show the enhancement of the decay rate (Purcell factor [57], $\mathcal{F}$) for the QE placed in the vicinity of GNRs. The plasmon modes of GNRs appear as resonant features in the calculated TDTB dependence of $\mathcal{F}$ on the transition frequency ω. These modes are labeled with the mode number p in order of increasing energy. The dipolar plasmon of the nanoribbon corresponds to $p = 1$. As follows from our results, the carbon atom vacancy introduced at the middle of the GNRs markedly changes the spectrum of the plasmon modes. Interestingly, only the plasmon modes with odd p are affected, while the modes with even p are insensitive to the presence of the vacancy. The vacancy effect is different depending on the type of GNR. For the AGNR-11 the plasmon modes with even p are blueshifted, while for the ZGNR-12 these modes are merely switched off.

To get insight into the observed trends let us recall that from the optical antenna theory [58,60,61], the plasmon modes of the defect-free GNRs correspond to the standing waves of the induced charges ρ_{ind} and currents I_{ind} having p half-wavelengths along the length L of the GNR. We define the induced current, $I_{\mathrm{ind}}(p, x)$, as the current associated with plasmon mode p and flowing through the nanoribbon cross section located at x. For the nanoantenna resonator $I_{\mathrm{ind}}(x, p) \propto \sin[\frac{\pi p}{L}(x + \frac{L}{2})]$. The plasmon modes with odd p possessing the nonzero dipole moment (or bright plasmon modes according to standard nomenclature) have antisymmetric charge density and symmetric current distribution along the nanoribbon x axis. The symmetries are reversed for the

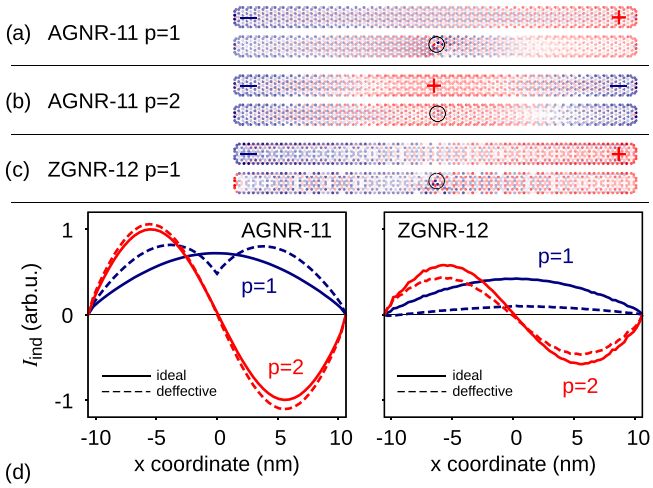

FIG. 3. Induced charges (a)–(c) and currents (d) associated with plasmon modes of the ideal and defective GNRs. The ZGNR-12 is electronically doped to Fermi energy $E_F = 0.4$ eV, while the AGNR-11 is neutral ($E_F = 0$). Position of the vacancy is indicated with a circle in panels (a)–(c), and it is defined in the caption of Fig. 2. (a)–(c) Upper (lower) image on each panel corresponds to an ideal (defective) GNR. The red (blue) color is used for the positive (negative) induced charge. In panel (d) the x-dependent induced current $I_{\mathrm{ind},p}(x)$ is shown for ideal (solid lines) and defective (dashed lines) GNRs.

dark (even p) plasmon modes, with no induced current flowing through the middle of the nanoribbon [see Figs. 2(e) and 2(f)]. It follows from our results that the vacancy placed at the middle of the nanoribbon perturbs the plasmon modes associated with maximum current flowing through its position. We thus infer that the modification of the plasmon modes is linked with the scattering of 2D electrons by the vacancy.

Consider an infinite defect-free AGNR-11. Its electronic structure corresponds to the continua of electronic states quantized in the transversal y direction and propagating in the longitudinal x direction [36,38,56,62,63]. For plasmon frequencies within a fraction of eV, the optical transitions involve the electronic bands closest to the Dirac point and thus characterized by the same transversal quantum number (see SM for the band structure). In this situation of the single transversal conductance channel, the vacancy positioned at line $N_v = 5$ at the middle of the L-long AGNR-11 efficiently reflects the optically excited electrons propagating along the GNR [25–27,37,43,64,65]. The vacancy-induced electron scattering effectively separates GNR into two parts. As follows from the induced charge density maps in Fig. 3, the dipolar plasmon ($p = 1$) of the L-long AGNR-11 with induced charges at nanoribbon extremities transforms into the analog of the bonding dipolar plasmon of the nearly touching dimer [8,66] of the $L/2$ AGNR-11. Indeed, the induced charges of opposite sign are accumulated across the vacancy region. The formation of a nonconductive junction is further evidenced by the dip in the current I_{ind} through the middle of the nanoribbon [see Fig. 3(d)], and it leads to the blueshift of the bright plasmon modes.

The dark plasmon modes of GNR with even p are characterized by a node of I_{ind} at $x = 0$ [see Fig. 3(d)]. Thus, these modes are basically insensitive to the vacancy located close to the middle of the GNR. Noteworthy, within the nearly touching dimer picture, the $p = 2$ mode of the L-long AGNR-11 transforms into the analog of the antibonding dipolar plasmon mode [8,66] of the $L/2$ dimer. This transformation does not involve a redistribution of the induced charges which keep the same sign across the nanoribbon cross section containing the vacancy [Fig. 3(b)]. In the SM we further discuss the evolution of the plasmon modes upon fusion of the dimer into a single nanoantenna.

The results shown in Figs. 3(c) and 3(d) for the electronically doped ZGNR-12, reveal a different situation. It can be related to the difference in the vacancy scattering of the 2D electrons moving within armchair and zigzag GNRs (for the detailed discussion of the scattering, see Ref. [25]). The electron reflection by the vacancy located on the $N_v = 6$ row at the middle of the ZGNR-12 is not sufficient to develop the nodal structure in I_{ind}, and to effectively split the nanoantenna into two parts [compare the blue dashed lines for $p = 1$ for AGNR-11 and ZGNR-12 in Fig. 3(d)]. The induced charges associated with plasmon modes have the same pattern for the ideal and defective nanoribbons. However, the coherent electron transport through the middle of the junction is strongly perturbed, leading to an efficient broadening and quenching of the bright plasmon modes [67,68]. This is while, as explained above, the dark plasmon modes are basically not affected by the vacancy.

It is worth noting that the strong plasmon reflection has been reported for the nanometer-wide gaps in graphene monolayer [69]. As well, the blueshift of the dipolar plasmon energy and the dimer formation were reported for the transverse plasmon modes of wide nanoribbons upon removal of an entire carbon atom row in the longitudinal direction [70]. In our case, the defect is represented by the single atom vacancy.

To further explore the vacancy effect, we analyze in Fig. 4 the decay rate enhancement for the QE placed in the vicinity of graphene nanoantennas. The TDTB results are shown as a function of the transition frequency ω of the QE, for different lateral positions x_v of the vacancy. For fixed x_v, the decay rate enhancement as a function of ω features several resonances associated with plasmon modes of the nanoribbon. Changing the position of the carbon atom vacancy strongly modifies the energies and lifetimes of the plasmon modes, and thus has a prominent effect on the decay rate of the QE located near GNRs. One can control the dynamics of the QE exciton by single-atom manipulation within the nanoantenna.

We now turn to the general evolution of the plasmon modes with vacancy position x_v as revealed by Fig. 4. For the AGNR-11, the calculated trends can be understood considering the strong electron reflection by the vacancy which effectively decouples the electronic states located at both sides of the vacancy region. Thus, the L-long defective AGNR can be modeled by a dimer formed by two ideal AGNR-11 of lengths $L_1 = L/2 + x_v$ (white) and $L_2 = L/2 - x_v$ (green) separated by a nonconductive narrow junction as sketched in Fig. 4(a). Considering AGNR-11 antennas as resonators, for the particular vacancy positions $x_v = L[\frac{p_1}{p_1+p_2} - \frac{1}{2}]$, the p_1 mode of the L_1 nanoribbon and the p_2 mode of the L_2 nanoribbon are energy degenerate at ω_r. Their bonding and antibonding combinations are formed. Note that in this case the antibond-

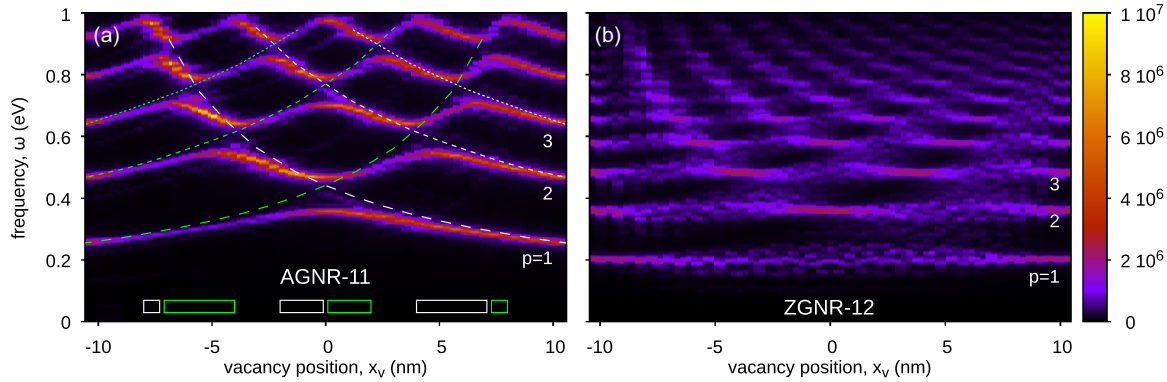

FIG. 4. The interpolated image of the decay rate enhancement $\mathcal{F} \times \omega^3$ given in eV^3 for the QE located in vicinity of the GNRs (see Fig. 1). The TDTB results for the AGNR-11 [panel (a)] and ZGNR-12 [panel (b)] are shown as a function of the transition frequency ω of the QE, and the vacancy position x_v. The color scale is given at the right of panel (b). The carbon atom vacancy is displaced following the fifth (sixth) atomic row for AGNR-11 (ZGNR-12). No charge doping is applied for AGNR-11 ($E_F = 0$), while the ZGNR is electronically doped to $E_F = 0.4$ eV. The plasmon resonances are labeled with their mode number p. The vacancy effectively splits the L-long AGNR-11 nanoantenna into the $L/2 + x_v$ (white rectangle) and $L/2 - x_v$ (green rectangle) dimer as sketched in the inset. The dotted lines show the plasmon resonance frequencies calculated with TDTB for individual AGNR-11 of the $L_1 = L/2 + x_v$ (white) and $L_2 = L/2 - x_v$ (green) lengths. Note that the high-frequency part of the data is presented for the sake of the discussion, and should be considered with care because of the strong optical phonon-induced plasmon broadening [18,45,68,71] not captured with TDTB. Note that the asymmetry of the panels with respect to the $x = 0$ vertical line results from the point dipole excitation with the point dipole located at the left side of the GNR (see Fig. 1).

ing combination is nothing else but the $p = p_1 + p_2$ mode of the AGNR at frequency ω_r. The coordinate x_v corresponds here to the node of its induced current where the induced charges are of the same sign across the vacancy position. In this situation one expects nearly no vacancy effect on the antibonding combination of p_1 (L_1) and p_2 (L_2) modes with its frequency close to ω_r.

The TDTB results corroborate the simple model outlined above. The calculated with TDTB x_v dependence of the resonance pattern in Fig. 4(a) indeed reveals an avoided crossing structure between the plasmon modes of the individual L_1 (L_2) -long nanoantennas. For the vacancy located at the node of the induced current of the plasmon mode $p = p_1 + p_2$ of the L-long nanoantenna, the avoided crossing between the p_1 (L_1) and p_2 (L_2) resonances results in formation of the (i) the slightly blueshifted antibonding-type resonance, and (ii) the bonding-type plasmon mode, whose energy is strongly redshifted with respect to ω.

In line with the results shown in Fig. 2, for the ZGNR-12 [Fig. 4(b)] the electron reflection by the vacancy is not sufficient to effectively produce a dimer configuration and to affect the energies of the plasmon modes. In this situation the loss of coherent electron transport and Landau damping associated with vacancy scattering results in the strong broadening and eventual quenching of the plasmon modes whenever the vacancy position is at the maximum of the induced current at $x_v = \frac{L}{2}[\frac{2n+1}{p} - 1]$, $0 \leqslant n < p$. At the same time, the plasmon modes (well-defined resonances of the Purcell factor) of the defect-free nanostructure are retrieved for x_v at the node of the induced current. The alternating maxima and minima of the induced current along the nanoribbon for different plasmon modes p is behind the pattern given by the broadening and narrowing of the plasmon resonances in Fig. 4(b).

We further demonstrate in the SM that the vacancy effect can be maximized or switched off not only by the longitudinal manipulation, but also by changing the transverse vacancy position given by atomic row N_v, and by the charge doping of GNR. As a result, with the same type of GNR, the vacancy can act on the plasmon modes as a "reflector" shifting the energy, as a "quencher" increasing the width, and as an "idler" which does not impact at all the plasmon response.

In conclusion, using the TDTB approach for graphene plasmonics we have demonstrated that a single carbon atom vacancy in the armchair and zigzag graphene nanoribbons comprising more than one thousand of carbon atoms leads to the prominent changes in the absorption spectra as well as in the decay rate of a quantum emitter coupled to a graphene nanoantenna. The underlying physical mechanism is a robust consequence of the strong defect-induced scattering of the optically excited electrons propagating along the narrow nanoribbon and it should hold for the systems with no strong electron interaction between GNRs and the substrate. Positioning the vacancy within the graphene lattice by using, e.g., a focused electron beam [72,73], allows for controllable energy shift and/or quenching of the given plasmon modes. Our work demonstrates that the link between the conductance of the optically excited electrons and the plasmon modes of the system [20–23,74,75] becomes particularly strong for the 2D materials. The findings reported in this work open a way for the atomic-scale design of the plasmonic 2D materials. As well, we envision that the strong sensitivity of the plasmon modes to the atomic-scale perturbations of the lattice can be used for the sensing applications.

[1] P. B. Corkum and F. Krausz, Attosecond science, Nat. Phys. **3**, 381 (2007).

[2] H. A. Atwater and A. Polman, Plasmonics for improved photovoltaic devices, Nat. Mater. **9**, 205 (2010).

[3] V. E. Ferry, L. A. Sweatlock, D. Pacifici, and H. A. Atwater, Plasmonic nanostructure design for efficient light coupling into solar cells, Nano Lett. **8**, 4391 (2008).

[4] S. Xiao, V. P. Drachev, A. V. Kildishev, X. Ni, U. K. Chettiar, H.-K. Yuan, and V. M. Shalaev, Loss-free and active optical negative-index metamaterials, Nature (London) **466**, 735 (2010).

[5] O. Hess, J. B. Pendry, S. A. Maier, R. F. Oulton, J. M. Hamm, and K. L. Tsakmakidis, Active nanoplasmonic metamaterials, Nat. Mater. **11**, 573 (2012).

[6] K. A. Willets and R. P. Van Duyne, Localized surface plasmon resonance spectroscopy and sensing, Annu. Rev. Phys. Chem. **58**, 267 (2007).

[7] D. Rodrigo, O. Limaj, D. Janner, D. Etezadi, F. J. García de Abajo, V. Pruneri, and H. Altug, Mid-infrared plasmonic biosensing with graphene, Science **349**, 165 (2015).

[8] N. J. Halas, S. Lal, W.-S. Chang, S. Link, and P. Nordlander, Plasmons in strongly coupled metallic nanostructures, Chem. Rev. **111**, 3913 (2011).

[9] K. L. Kelly, E. Coronado, L. L. Zhao, and G. C. Schatz, The optical properties of metal nanoparticles the influence of size, shape, and dielectric environment, J. Phys. Chem. B **107**, 668 (2003).

[10] S. Khatua, W.-S. Chang, P. Swanglap, J. Olson, and S. Link, Active modulation of nanorod plasmons, Nano Lett. **11**, 3797 (2011).

[11] W. M. Wilson, J. W. Stewart, and M. H. Mikkelsen, Surpassing single line width active tuning with photochromic molecules coupled to plasmonic nanoantennas, Nano Lett. **18**, 853 (2018).

[12] L. Polavarapu and L. M. Liz-Marzán, Towards low-cost flexible substrates for nanoplasmonic sensing, Phys. Chem. Chem. Phys. **15**, 5288 (2013).

[13] D. Yoo, T. W. Johnson, S. Cherukulappurath, D. J. Norris, and S.-H. Oh, Template-stripped tunable plasmonic devices on stretchable and rollable substrates, ACS Nano **9**, 10647 (2015).

[14] P. Mulvaney, J. Pérez-Juste, M. Giersig, L. M. Liz-Marzán, and C. Pecharromán, Drastic surface plasmon mode shifts in gold nanorods due to electron charging, Plasmonics **1**, 61 (2006).

[15] Y. Li, J. van de Groep, A. A. Talin, and M. L. Brongersma, Dynamic tuning of gap plasmon resonances using a solid-state electrochromic device, Nano Lett. **19**, 7988 (2019).

[16] F. H. L. Koppens, D. E. Chang, and F. J. García de Abajo, Graphene plasmonics: A platform for strong light-matter interactions, Nano Lett. **11**, 3370 (2011).

[17] A. N. Grigorenko, M. Polini, and K. S. Novoselov, Graphene plasmonics, Nat. Photonics **6**, 749 (2012).

[18] T. Low and P. Avouris, Graphene plasmonics for terahertz to mid-infrared applications, ACS Nano **8**, 1086 (2014).

[19] F. J. García de Abajo, Graphene plasmonics: Challenges and opportunities, ACS Photonics **1**, 135 (2014).

[20] P. Song, P. Nordlander, and S. Gao, Quantum mechanical study of the coupling of plasmon excitations to atomic-scale electron transport, J. Chem. Phys. **134**, 074701 (2011).

[21] A. Emboras, J. Niegemann, P. Ma, C. Haffner, A. Pedersen, M. Luisier, C. Hafner, T. Schimmel, and J. Leuthold, Atomic scale plasmonic switch, Nano Lett. **16**, 709 (2016).

[22] T. P. Rossi, A. Zugarramurdi, M. J. Puska, and R. M. Nieminen, Quantized Evolution of the Plasmonic Response in a Stretched Nanorod, Phys. Rev. Lett. **115**, 236804 (2015).

[23] F. Marchesin, P. Koval, M. Barbry, J. Aizpurua, and D. Sánchez-Portal, Plasmonic response of metallic nanojunctions driven by single atom motion: Quantum transport revealed in optics, ACS Photonics **3**, 269 (2016).

[24] B. Biel, F. Triozon, X. Blase, and S. Roche, Chemically induced mobility gaps in graphene nanoribbons: A route for upscaling device performances, Nano Lett. **9**, 2725 (2009).

[25] H.-Y. Deng and K. Wakabayashi, Vacancy effects on electronic and transport properties of graphene nanoribbons, Phys. Rev. B **91**, 035425 (2015).

[26] D. A. Bahamon, A. L. C. Pereira, and P. A. Schulz, Tunable resonances due to vacancies in graphene nanoribbons, Phys. Rev. B **82**, 165438 (2010).

[27] I. Deretzis, G. Fiori, G. Iannaccone, and A. La Magna, Effects due to backscattering and pseudogap features in graphene nanoribbons with single vacancies, Phys. Rev. B **81**, 085427 (2010).

[28] J. Haskins, A. Kınacı, C. Sevik, H. Sevinçli, G. Cuniberti, and T. Çağin, Control of thermal and electronic transport in defect-engineered graphene nanoribbons, ACS Nano **5**, 3779 (2011).

[29] W. Han, R. K. Kawakami, M. Gmitra, and J. Fabian, Graphene spintronics, Nat. Nanotechnol. **9**, 794 (2014).

[30] O. V. Yazyev and L. Helm, Defect-induced magnetism in graphene, Phys. Rev. B **75**, 125408 (2007).

[31] N. Friedrich, P. Brandimarte, J. Li, S. Saito, S. Yamaguchi, I. Pozo, D. Peña, T. Frederiksen, A. Garcia-Lekue, D. Sánchez-Portal, and J. I. Pascual, Magnetism of Topological Boundary StatesInduced by Boron Substitution in Graphene Nanoribbons, Phys. Rev. Lett. **125**, 146801 (2020).

[32] F. Lombardi, A. Lodi, J. Ma, J. Liu, M. Slota, A. Narita, W. K. Myers, K. Müllen, X. Feng, and L. Bogani, Quantum units from the topological engineering of molecular graphenoids, Science **366**, 1107 (2019).

[33] In order to account for the plasmon decay channels beyond the TDTB description, the spectral structures are artificially broadened with the broadening γ. In particular, the plasmon modes with energies above ($\Omega = 0.2$ eV) might experience strong broadening 30–40 meV because of the plasmon decay assisted by the optical phonon excitation. However, for the sake of the clear-cut presentation of the vacancy effect we prefer to use in the main text of the paper $\gamma = 5$ meV, and to explicitly show in the SM that our main results are robust and hold for $\gamma = 30$ meV.

[34] F. Banhart, J. Kotakoski, and A. V. Krasheninnikov, Structural defects in graphene, ACS Nano **5**, 26 (2011).

[35] H. Terrones, R. Lv, M. Terrones, and M. S. Dresselhaus, The role of defects and doping in 2D graphene sheets and 1D nanoribbons, Rep. Prog. Phys. **75**, 062501 (2012).

[36] L. E. F. Foa Torres, S. Roche, and J.-C. Charlier, *Introduction to Graphene-Based Nanomaterials: From Electronic Structure to Quantum Transport*, 2nd ed. (Cambridge University Press, Cambridge, UK, 2020), pp. 11–69.

[37] K. Wakabayashi, Numerical study of the lattice vacancy effects on the single-channel electron transport of graphite ribbons, J. Phys. Soc. Jpn. **71**, 2500 (2002).

[38] K. Wakabayashi, Y. Takane, M. Yamamoto, and M. Sigrist, Electronic transport properties of graphene nanoribbons, New J. Phys. **11**, 095016 (2009).

[39] K. Kaasbjerg, Atomistic t-matrix theory of disordered two-dimensional materials: Bound states, spectral properties, quasiparticle scattering, and transport, Phys. Rev. B **101**, 045433 (2020).

[40] V. M. Pereira, J. M. B. Lopes dos Santos, and A. H. Castro Neto, Modeling disorder in graphene, Phys. Rev. B **77**, 115109 (2008).

[41] S. Yuan, R. Roldán, H. De Raedt, and M. I. Katsnelson, Optical conductivity of disordered graphene beyond the Dirac cone approximation, Phys. Rev. B **84**, 195418 (2011).

[42] T. Stauber, N. M. R. Peres, and F. Guinea, Electronic transport in graphene: A semiclassical approach including midgap states, Phys. Rev. B **76**, 205423 (2007).

[43] Z. Kan, M. Khatun, and A. Cancio, Quantum transport in zigzag graphene nanoribbons in the presence of vacancies, J. Appl. Phys. **125**, 164305 (2019).

[44] C. Vacacela Gomez, M. Pisarra, M. Gravina, J. M. Pitarke, and A. Sindona, Plasmon Modes of Graphene Nanoribbons with Periodic Planar Arrangements, Phys. Rev. Lett. **117**, 116801 (2016).

[45] F. Karimi and I. Knezevic, Plasmons in graphene nanoribbons, Phys. Rev. B **96**, 125417 (2017).

[46] K. O. Wedel, N. A. Mortensen, K. S. Thygesen, and M. Wubs, Emergent scale invariance of nonclassical plasmons in graphene nanoribbons, Phys. Rev. B **98**, 155412 (2018).

[47] C. E. P. Villegas, M. R. S. Tavares, G.-Q. Hai, and P. Vasilopoulos, Plasmon modes and screening in double metallic armchair graphene nanoribbons, Phys. Rev. B **88**, 165426 (2013).

[48] L. Brey and H. A. Fertig, Elementary electronic excitations in graphene nanoribbons, Phys. Rev. B **75**, 125434 (2007).

[49] A. A. Shylau, S. M. Badalyan, F. M. Peeters, and A. P. Jauho, Electron polarization function and plasmons in metallic armchair graphene nanoribbons, Phys. Rev. B **91**, 205444 (2015).

[50] D. R. Andersen and H. Raza, Plasmon dispersion in semimetallic armchair graphene nanoribbons, Phys. Rev. B **85**, 075425 (2012).

[51] F. Hu, Y. Luan, Z. Fei, I. Z. Palubski, M. D. Goldflam, S. Dai, J.-S. Wu, K. W. Post, G. C. A. M. Janssen, M. M. Fogler, and D. N. Basov, Imaging the localized plasmon resonance modes in graphene nanoribbons, Nano Lett. **17**, 5423 (2017).

[52] See Supplemental Material at http://link.aps.org/supplemental/10.1103/PhysRevB.105.L081401 for the brief description of the time-dependent tight-binding approach; discussion of the robust character of the results with respect to the plasmon mode broadening because of the coupling to optical phonons; analysis of the evolution of the plasmon modes for the separated nanoribbon dimer upon the closing of the dimer gap; electronic band structure of the infinite AGNR-11 and ZGNR-12 nanoribbons; dependence of the optical response of the nanoribbon on the transversal displacement of the vacancy (the effect of the choice of the carbon atom row) and on the electronic doping given by the Fermi energy; and analysis of the transition to the wide ribbon limit.

[53] J. D. Cox, I. Silveiro, and F. J. García de Abajo, Quantum effects in the nonlinear response of graphene plasmons, ACS Nano **10**, 1995 (2016).

[54] S. Thongrattanasiri, A. Manjavacas, and F. J. García de Abajo, Quantum finite-size effects in graphene plasmons, ACS Nano **6**, 1766 (2012).

[55] F. Aguillon, D. C. Marinica, and A. G. Borisov, Molecule detection with graphene dimer nanoantennas, J. Phys. Chem. C **124**, 28210 (2020).

[56] K. Wakabayashi, K. ichi Sasaki, T. Nakanishi, and T. Enoki, Electronic states of graphene nanoribbons and analytical solutions, Sci. Technol. Adv. Mater. **11**, 054504 (2010).

[57] L. Novotny and B. Hecht, *Principles of Nano-Optics* (Cambridge University Press, Cambridge, UK, 2006).

[58] P. Bharadwaj, B. Deutsch, and L. Novotny, Optical antennas, Adv. Opt. Photonics **1**, 438 (2009).

[59] R. Carminati, A. Cazé, D. Cao, F. Peragut, V. Krachmalnicoff, R. Pierrat, and Y. De Wilde, Electromagnetic density of states in complex plasmonic systems, Surf. Sci. Rep. **70**, 1 (2015).

[60] L. Novotny and N. van Hulst, Antennas for light, Nat. Photonics **5**, 83 (2011).

[61] P. Biagioni, J.-S. Huang, and B. Hecht, Nanoantennas for visible and infrared radiation, Rep. Prog. Phys. **75**, 024402 (2012).

[62] L. Brey and H. A. Fertig, Electronic states of graphene nanoribbons studied with the Dirac equation, Phys. Rev. B **73**, 235411 (2006).

[63] H. Zheng, Z. F. Wang, T. Luo, Q. W. Shi, and J. Chen, Analytical study of electronic structure in armchair graphene nanoribbons, Phys. Rev. B **75**, 165414 (2007).

[64] N. Gorjizadeh, A. A. Farajian, and Y. Kawazoe, The effects of defects on the conductance of graphene nanoribbons, Nanotechnology **20**, 015201 (2008).

[65] T. C. Li and S.-P. Lu, Quantum conductance of graphene nanoribbons with edge defects, Phys. Rev. B **77**, 085408 (2008).

[66] P. Nordlander, C. Oubre, E. Prodan, K. Li, and M. I. Stockman, Plasmon hybridization in nanoparticle dimers, Nano Lett. **4**, 899 (2004).

[67] A. Principi, G. Vignale, M. Carrega, and M. Polini, Impact of disorder on Dirac plasmon losses, Phys. Rev. B **88**, 121405(R) (2013).

[68] M. Jablan, H. Buljan, and M. Soljačić, Plasmonics in graphene at infrared frequencies, Phys. Rev. B **80**, 245435 (2009).

[69] J. Chen, M. L. Nesterov, A. Y. Nikitin, S. Thongrattanasiri, P. Alonso-González, T. M. Slipchenko, F. Speck, M. Ostler, T. Seyller, I. Crassee, F. H. L. Koppens, L. Martin-Moreno, F. J. García de Abajo, A. B. Kuzmenko, and R. Hillenbrand, Strong plasmon reflection at nanometer-size gaps in monolayer graphene on SiC, Nano Lett. **13**, 6210 (2013).

[70] I. Silveiro, J. M. P. Ortega, and F. J. G. de Abajo, Quantum nonlocal effects in individual and interacting graphene nanoribbons, Light: Sci. Appl. **4**, e241 (2015).

[71] D. Novko, Dopant induced plasmon decay in graphene, Nano Lett. **17**, 6991 (2017).

[72] A. W. Robertson, C. S. Allen, Y. A. Wu, K. He, J. Olivier, J. Neethling, A. I. Kirkland, and J. H. Warner, Spatial control of

defect creation in graphene at the nanoscale, Nat. Commun. **3**, 1144 (2012).

[73] M. H. Rummeli, H. Q. Ta, R. G. Mendes, I. G. Gonzalez-Martinez, L. Zhao, J. Gao, L. Fu, T. Gemming, A. Bachmatiuk, and Z. Liu, New frontiers in electron beam-driven chemistry in and around graphene, Adv. Mater. **31**, 1800715 (2019).

[74] G. Di Martino, S. Tappertzhofen, S. Hofmann, and J. Baumberg, Nanoscale plasmon-enhanced spectroscopy in memristive switches, Small **12**, 1334 (2016).

[75] P. Garcia-Gonzalez, A. Varas, F. Garcia-Vidal, and A. Rubio, Single-atom control of the optoelectronic response in sub-nanometric cavities, arXiv:1903.08443.